GEOPHYSICS, VOL. 67, NO. 3 (MAY-JUNE 2002); P. 727–738, 12 FIGS., 1 TABLE.
10.1190/1.1484515

Dielectric permittivity and resistivity mapping using high-frequency, helicopter-borne EM data

Haoping Huang* and Douglas C. Fraser‡

ABSTRACT

The interpretation of helicopter-borne electromagnetic (EM) data is commonly based on the transformation of the data to the apparent resistivity under the assumption that the dielectric permittivity is that of free space and so displacement currents may be ignored. While this is an acceptable approach for many applications, it may not yield a reliable value for the apparent resistivity in resistive areas at the high frequencies now available commercially for some helicopter EM systems.

We analyze the feasibility of mapping spatial variations in the dielectric permittivity and resistivity using a high-frequency helicopter-borne EM system. The effect of the dielectric permittivity on the EM data is to decrease the in-phase component and increase the quadrature component. This results in an unwarranted increase in the apparent resistivity (when permittivity is neglected) for the pseudolayer half-space model, or a decrease in the apparent resistivity for the homogeneous half-space model. To avoid this problem, we use the in-phase and quadrature responses at the highest frequency to estimate the apparent dielectric permittivity because this maximizes the response of displacement currents. Having an estimate of the apparent dielectric permittivity then allows the apparent resistivity to be computed for all frequencies. A field example shows that the permittivity can be well resolved in a resistive environment when using high-frequency helicopter EM data.

INTRODUCTION

Helicopter electromagnetic (EM) methods are used both for conductive target detection and for general purpose mapping of electrical properties. For target detection, the EM data are often interpreted in terms of a vertical dike model with the conductance (or conductivity-thickness product) being presented as anomaly symbols on a map. For electrical mapping, the data are commonly transformed to the conductivity or the resistivity (= conductivity^{-1}) of a half-space model under the assumption that magnetic permeability is that of free space and the frequency is sufficiently low that dielectric permittivity may be ignored (Fraser, 1978; Sengpiel, 1988; Huang and Fraser, 1996). However, a modern multifrequency EM system may operate at sufficiently high frequencies that the dielectric response is observable in the data. The apparent resistivity (or conductivity) obtained from the EM data over a dielectrically polarizable earth may be biased if the displacement currents are ignored in the analysis.

The recent development of a specialized helicopter EM system for mapping resistivity, called DIGHEM$^{V}_{Res}$, employs only horizontal coplanar transmitting-receiving coil-pairs. The separation between the centers of the transmitting and receiving coils is 7.92 m. There are five geometrically spaced frequencies with the lowest and highest frequencies, respectively, being 380 and 105 000 Hz. In resistive areas, the highest frequency allows the mapping of the dielectric permittivity. In conductive areas, the skin depth phenomenon at the highest frequency limits the depth of investigation to the upper few meters while the low frequencies explore deeper. The shallow information is desirable for many environmental and engineering problems, and also provides near-surface resistivities to aid in the inversion for conductors at depth.

Information on the dielectric permittivity of the earth may be useful in problems of electric power transmission, geological mapping, and environmental pollution. Dielectric permittivity mapping can be particularly important for hazardous waste site characterization because some contaminants may have little effect on observed resistivity but a large effect on observed permittivity (Olhoeft, 1986).

Many researchers have recognized the existence of or dealt with dielectric permittivity in EM data. For example, Sinha (1977) presented a graphical means for obtaining resistivity

Published on Geophysics Online October 29, 2001. Manuscript received by the Editor June 23, 1999; revised manuscript received May 31, 2001.
*Formerly Geoterrex-Dighem, Unit 2, 2270 Argentia Road, Mississauga, Ontario L5N 6A6, Canada; presently Geophex, Limited, 605 Mercury Street, Raleigh, North Carolina 27603. E-mail: huang@geophex.com.
‡Formerly Geoterrex-Dighem, Unit 2, 2270 Argentia Road, Mississauga, Ontario L5N 6A6, Canada; presently a consultant, 1294 Gatehouse Drive, Mississauga, Ontario L5H 1A5, Canada. E-mail: dougfraser1@cs.com.

and dielectric permittivity from plane-wave EM fields. Lytle et al. (1976) used the oscillatory behavior of the wave tilt at high frequencies to resolve layer thickness. Stewart et al. (1994) demonstrated the influence of dielectric properties on layered-earth measurements for a high-frequency ground EM system. Song et al. (1997) presented methods for evaluating the incident angle, correcting the impedance data for normal incidence, and imaging the conductivity and permittivity of layered earth models for a high-frequency plane-wave ground EM system. While Fraser et al. (1990) analyzed the magnitude of the response of displacement currents on the dipole-dipole data from a high-frequency helicopter EM system, no attempt was made to correct the estimated resistivity by employing a precomputed value for the dielectric permittivity. Based on a homogeneous half-space model, they observed that the error in the estimated resistivity can exceed 10% when the ignored displacement currents exceed 5% of the amplitude of conduction currents. This situation occurs, for example, over a 2000 ohm-m half-space for a frequency of 50 000 Hz when the relative dielectric permittivity is 10.

Huang and Fraser (2001) developed a means of obtaining simultaneously the resistivity, magnetic permeability, and dielectric permittivity from a transformation of multifrequency helicopter EM data. However, in the absence of magnetically permeable earth materials in the survey area, the resistivity and dielectric permittivity can be obtained more accurately and quickly by eliminating the permeability variable in the equations and corresponding lookup table. This present paper continues the development by Huang et al. (1998) for mapping the responses of the dielectric permittivity and conductivity in resistive areas, assuming the magnetic permeability is that of free space. As for Fraser (1978) and Huang and Fraser (2000, 2001), we deal with both the homogeneous half-space model (Figure 1a) and the pseudolayer half-space model (Figure 1b). For forward solutions, these models are identical since the thickness t of the pseudo-layer in Figure 1b is set to zero. For inverse and transform solutions, the models differ inasmuch as the homogeneous half-space of Figure 1a uses the EM amplitude and altimeter as input to compute the apparent resistivity, whereas the pseudolayer model of Figure 1b uses the EM amplitude and phase (or, equally, the in-phase and quadrature) to compute both the apparent resistivity and the apparent sensor altitude.

We provide synthetic and field examples to show the impact of the dielectric permittivity on the computed resistivity. While the technique is applicable to any closely-coupled airborne EM system, we specifically employ the highest frequency of 105 000 Hz from the new DIGHEM$^{V}_{Res}$ coplanar-coil resistivity mapping system for the synthetic examples, while showing a field example for 56 000 Hz from the older DIGHEM^{V} coaxial-coil/coplanar-coil system.

With the availability of a variety of inversion techniques, the reader might wonder why we choose to develop transforms. The reason is one of computational speed. The transform described below requires less than 1/30th the time of an inversion to a half-space, an important issue when dealing with large volumes of airborne survey data.

CURRENT FLOW IN EARTH MATERIALS

The primary magnetic field of an airborne electromagnetic transmitting coil produces current flow in the earth (e.g., Ward,

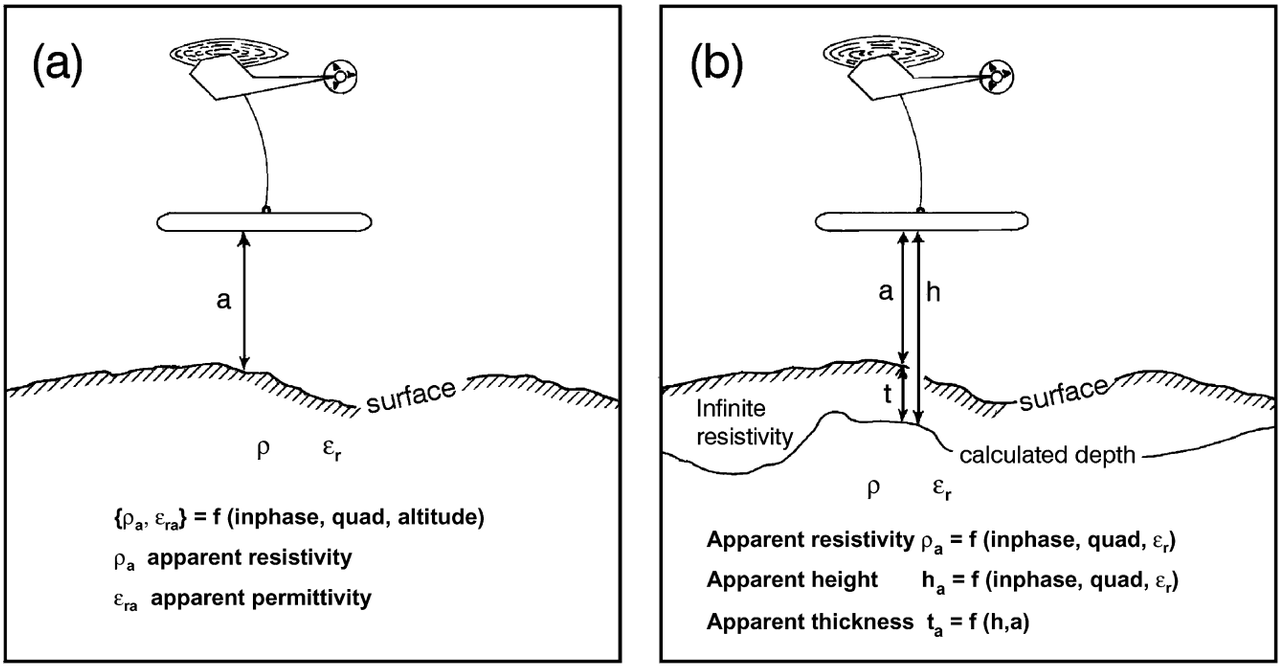

FIG. 1. (a) The homogeneous half-space model, where the top of the half-space coincides with the earth's surface as defined by the radar or laser altimeter. (b) The pseudolayer half-space model, where the top of the half-space is defined numerically by the output parameter h. The pseudolayer half-space model is equivalent to a two-layer case where the upper layer is of infinite resistivity. The thickness t is the difference between the interpreted sensor-source height h and the bird altitude a as obtained from the altimeter.

1967; Lysne, 1983; Wait, 1984; Ward and Holmann, 1988). The total current flow $\mathbf{J}_T$ is the sum of the conduction current $\sigma\mathbf{E}$ and the displacement current $i\omega\varepsilon\mathbf{E}$, i.e.,

$$\mathbf{J}_T = \sigma\mathbf{E} + i\omega\varepsilon\mathbf{E} = (\sigma + i\omega\varepsilon)\mathbf{E} \tag{1}$$

for a source field varying harmonically at the angular frequency ω, where $\mathbf{E}$ is the electric field intensity, i is the imaginary number, σ is the conductivity, and ε is the dielectric permittivity. At low frequency, in the absence of magnetic rocks, any current flow will primarily be due to conduction. At higher frequencies, displacement currents also may be of importance.

In applied geophysics, we often deal with the resistivity

$$\rho = \frac{1}{\sigma} \tag{2}$$

and the relative dielectric permittivity (dielectric constant)

$$\varepsilon_r = \frac{\varepsilon}{\varepsilon_0}, \tag{3}$$

where ε_0 is the dielectric permittivity of free space and where it is assumed that conductivity and permittivity are frequency independent.

In the design of EM systems, the angular frequency ω of the transmitting coil has historically been kept sufficiently low such that $\sigma \gg \omega\varepsilon$. The purpose of this is to avoid generating displacement currents because the primary property of interest is the conductivity. This condition reduces equation (1) to

$$\mathbf{J}_T = \sigma\mathbf{E}. \tag{4}$$

This quasi-static assumption can lead to substantial errors when analyzing the EM data for frequencies greater than 10 000 Hz.

A useful representation for defining the response of a dielectric conductive half-space is the dimensionless response parameter θ^2 (Grant and West, 1965). For the half-space, we have

$$\theta^2 = (\omega^2\varepsilon\mu - i\omega\sigma\mu)h^2 = \omega^2\varepsilon\mu h^2 - i\omega\sigma\mu h^2 = \alpha - i\beta, \tag{5}$$

where h is the sensor-source height (Figure 1b), and α and β are, respectively, the dielectric part and the conductive part of the response parameter. In the quasi-static assumption, α is set to zero rather than to the free space condition of $\omega^2\varepsilon_0\mu_0 h^2$.

THE EFFECT OF DISPLACEMENT CURRENTS

For closely coupled transmitting and receiving coils, as exists in frequency-domain helicopter EM systems, the ratio of the secondary magnetic field intensity H_s to the primary magnetic field intensity H_0 at the receiving coil can be approximated for the quasi-static case as (Fraser, 1972)

$$\frac{H_s}{H_0} = (s/h)^3[M + iN]. \tag{6}$$

The measured in-phase I and quadrature Q components of the EM amplitude may be represented as

$$I = (s/h)^3 M \quad \text{and} \quad Q = (s/h)^3 N, \tag{7}$$

where the I and Q components are expressed in units of parts per million (ppm) of the primary magnetic field intensity H_0 at the receiving coil. M and N are a function of the complex induction number θ, and portray the in-phase and quadrature response normalized for variations in flying height h and coil separation s. Equations (6) and (7) are valid when $s^3 \ll h^3$. This superimposed dipole assumption (Grant and West, 1965) is generally valid for surveys flown with frequency-domain helicopter EM systems.

To illustrate the effect of displacement currents at high frequencies, the in-phase I and quadrature Q components were computed for a variety of dielectric conductive half-spaces (Figures 2a, 2b). The resistivities range from 10^2 to 10^6 ohm-m, and the relative dielectric permittivities range from 0 to 80. The value of 0 for the relative dielectric permittivity indicates the quasi-static case where the displacement current is not taken into account [i.e., $\alpha = 0$ in equation (5)]. It is evident from Figures 2a and 2b that displacement currents may modify the in-phase and quadrature responses noticeably from the conduction current responses for a half-space resistivity above 1000 ohm-m for this frequency of 105 000 Hz.

Displacement currents are 90° out-of-phase with conduction currents as indicated by equation (1). In accordance with the common signing convention for helicopter EM data, displacement currents yield negative in-phase and positive quadrature components. These add to the positive in-phase and positive quadrature components from conduction currents. Displacement currents therefore result in a smaller in-phase (Figure 2a) and a larger quadrature (Figure 2b) than would be the case in their absence. These changes to the observed EM responses bias the computed apparent resistivity if displacement currents are ignored. Specifically, the computed resistivity will be erroneously high for the pseudolayer half-space model (Figure 2c) while being erroneously low for the homogeneous half-space model (Figure 2d).

DETERMINATION OF APPARENT PERMITTIVITY AND RESISTIVITY

The dielectric permittivity and conductivity of a dielectric conductive half-space are obtained by transforming the in-phase and quadrature responses using a table lookup program that yields the same results as a one-layer inversion. However, the computation is much more efficient than inversion since an iterative method is not employed. We describe the lookup procedure in the Appendix and demonstrate the method graphically by the use of Figure 3.

Determination of the apparent relative permittivity

To calculate the apparent permittivity, the normalized in-phase M and quadrature N components are first obtained from the measured in-phase I and quadrature Q components from equation (7) for a specific frequency, on the assumption that the bird altitude a can be used in place of the unknown sensor-source height h. The relative dielectric permittivity is then obtained by locating the M', N position on Figure 3, which is the phasor diagram for the half-space model of a dielectric conductive earth for the same frequency. This diagram yields the real $\alpha = \omega^2\varepsilon_r\varepsilon_0\mu h^2$ and imaginary $\beta = \omega\mu\sigma h^2$ components of the complex response parameter θ^2 given the quantities M' and N. M' is simply M plus the base value of 20 000 added to keep this quantity positive for display purposes. The relative dielectric permittivity is then obtained from the real component α of θ^2 as

$$\varepsilon_r = \frac{\alpha}{\omega^2 \varepsilon_0 \mu h^2}, \tag{8}$$

where the free space value of μ_0 is used for μ.

The imaginary component β of the response parameter θ^2 may also be obtained from Figure 3. It serves as an indication of the resolvability of the relative dielectric permittivity. If β is less than 1, the value of ε_r from Figure 3 and equation (8) is likely to be reliable. If β is greater than 1, α is poorly resolved, and so the relative permittivity ε_r will be unreliable. In practice, the above procedure should be followed using data from the highest frequency to maximize the response of displacement currents. With a resistivity of 1000 ohm-m, a relative magnetic permeability of free space, and a frequency of 100 000 Hz, the imaginary component β of the response parameter is 0.97 for a sensor altitude of 35 m (the normal survey altitude is 30–35 m). Thus, the condition $\beta < 1$ should be satisfied for this frequency if a survey environment is more resistive than 1000 ohm-m. Certainly, Figure 3 is generally applicable for DIGHEM surveys in the resistive Precambrian Shield environments of Scandinavia and northern Canada, including the great Canadian diamond play at Lac de Gras in the Northwest Territories, where resistivities commonly exceed 10 000 ohm-m.

Determination of the apparent resistivity

The apparent resistivity can be determined from the measured in-phase and quadrature components for each individual frequency following the above computation of the relative dielectric permittivity ε_r. The resistivity can be computed using either the homogeneous half-space model of Figure 1a or the pseudolayer half-space model of Figure 1b.

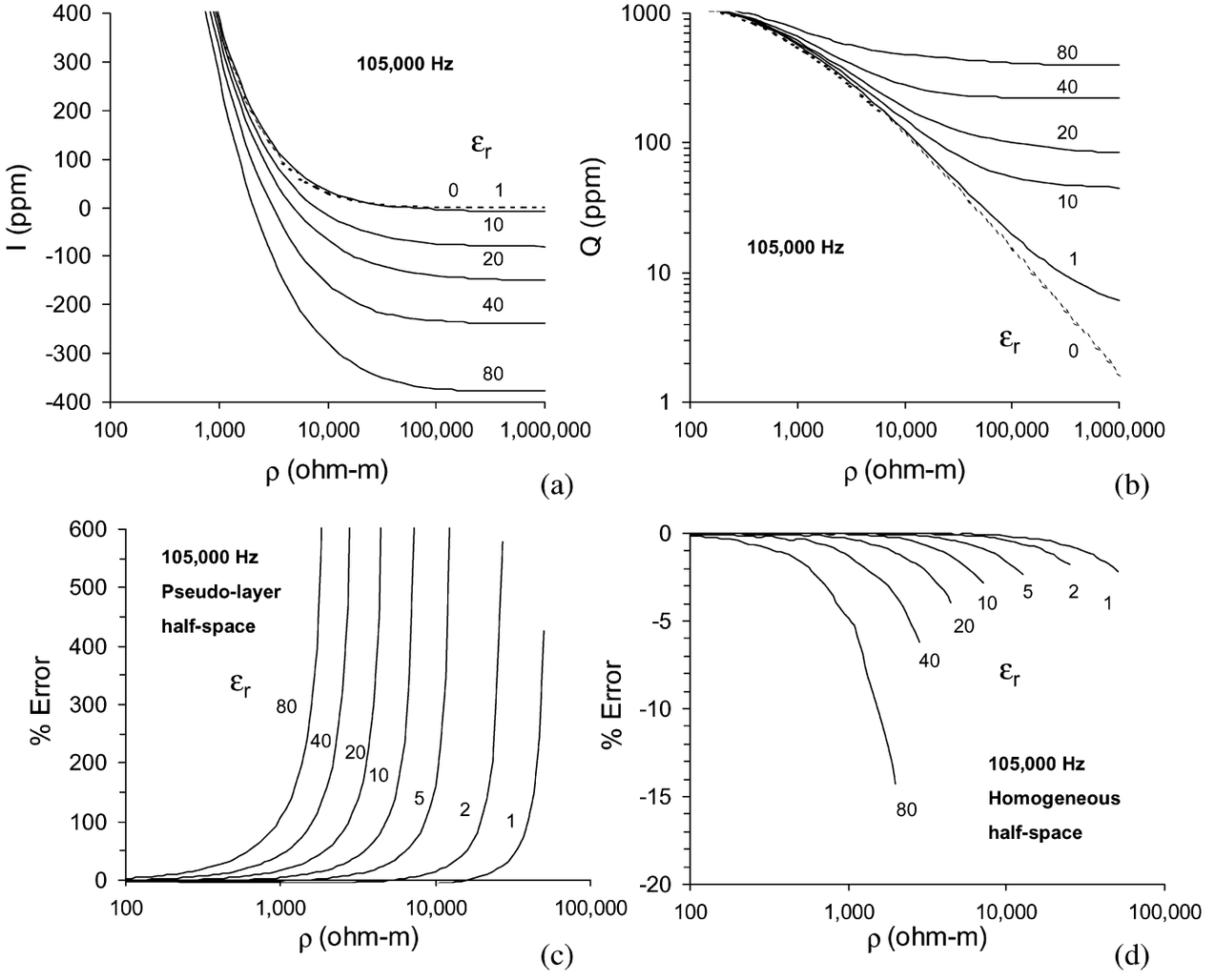

FIG. 2. The (a) in-phase I and (b) quadrature Q responses in ppm from a horizontal coplanar coil-pair, as a function of resistivity ρ, for various relative dielectric permittivities ε_r. The frequency is 105 000 Hz, the transmitting-receiving coil separation is 7.92 m, and the flying height is 30 m. (c) Percent error in the computed resistivity using the pseudolayer half-space model when displacement currents are ignored. (d) Percent error in the computed resistivity using the homogeneous half-space model when displacement currents are ignored. The percent error is not shown when the in-phase component is negative because the resistivity is not physically meaningful for negative in-phase when displacement currents are ignored.

If the homogeneous half-space model is used, the resistivity for the highest frequency, which was used to compute the dielectric permittivity, can be obtained directly from the β of Figure 3, i.e.,

$$\rho_a = \frac{\omega\mu h^2}{\beta}, \tag{9}$$

where ρ_a is the apparent resistivity and where h is set equal to the EM sensor altitude a as obtained from the altimeter, and the magnetic permeability $\mu = \mu_0$.

Equations (8) and (9) can be expressed conceptually as

$$\{\varepsilon_r, \rho\} = \Phi(M, N, a), \tag{10}$$

where Φ is the homogeneous half-space operator (which employs the table lookup program) equivalent to Figure 3, and where the inputs are the normalized in-phase M and quadrature N, and the altitude a. Since the apparent dielectric permittivity determined from the highest frequency is likely to be more reliable than those obtained from lower frequencies, we use it to compute the apparent resistivities for the other frequencies. We use an algorithm similar to equation (10) except that ε_r is fixed.

On the other hand, if the pseudolayer half-space model (Figure 1b) is used, the apparent resistivity is computed using the same imaginary component β in equation (9), but h is used for the sensor-source distance rather than a (Figure 1). The equivalent algorithm can be written conceptually as

$$\{\rho, h\} = \Gamma(M, N, \varepsilon_r), \tag{11}$$

where the input ε_r is obtained from equation (8), and Γ is the operator equivalent to that developed by Fraser (1978) for the quasi-static case but with a finite value for the relative dielectric permittivity ε_r. The apparent thickness of the pseudolayer (Figure 1b) is calculated from the apparent height h_a and the altimeter value a as

$$t_a = h_a - a. \tag{12}$$

Our algorithm was tested on synthetic, noise-free data from a dielectric conductive half-space for a number of forward models with relative permittivities ε_r ranging from 1 to 80 and with resistivities ranging from 10^2 to 10^6 ohm-m. These models were used to compute the in-phase I and quadrature Q components for a frequency of 105 000 Hz and an EM bird height of 30 m. The in-phase and quadrature components were then used to estimate the resistivities and the relative dielectric permittivities. Table 1 shows that the solutions to the relative permittivity match the forward models almost exactly for resistivities above 1000 ohm-m. When the resistivity is 100 ohm-m, the condition $\sigma \gg \omega\varepsilon$ is satisfied, so the relative permittivity cannot be resolved. The resistivity solution is reasonable for this noise-free synthetic data for all values of the relative permittivity, and is independent of the permittivity when the conductivity $\sigma \gg \omega\varepsilon$.

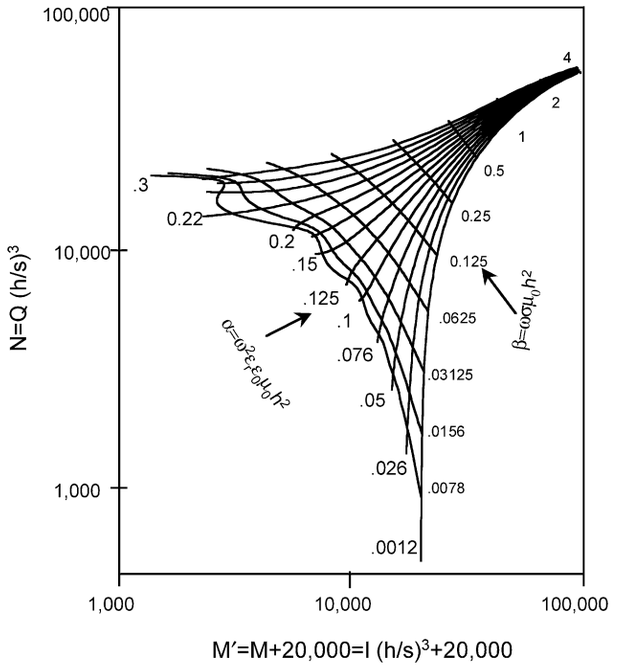

FIG. 3. Phasor diagram of the normalized in-phase M' and quadrature N components for the half-space model for several resistivities ρ and relative permittivities ε_r. M' is taken as $M + 20\,000$ to allow negative values of M to be portrayed in log-space. A frequency of 56 000 Hz was used.

APPARENT RESISTIVITY AND PERMITTIVITY FOR LAYERED EARTHS

We now discuss the behavior of the apparent relative permittivity and apparent resistivity for layered earth models. The in-phase and quadrature amplitudes are computed from the models for a frequency of 105 000 Hz, and then used as inputs to the permittivity-resistivity algorithm.

Figure 4a presents a two-layer model where the thickness t_1 of the upper layer is variable. The relative dielectric

Table 1. The computed apparent relative permittivity ε_{ra} and apparent resistivity ρ_a for dielectric conductive half-space models using the permittivity-resistivity inversion algorithm. The dash indicates there is no solution. Resistivity is in ohm-meters.

True ρ	100		1000		10 000		100 000		1 000 000	
True ε_r	ε_{ra}	ρ_a	ε_{ra}	ρ_a	ε_{ra}	ρ_a	ε_{ra}	ρ_a	ε_{ra}	ρ_a
1	–	100	1.000	1000	1.000	10 000	1.003	100 012	1.000	991 019
2	–	100	2.031	1000	2.003	9 999	1.998	99 892	1.998	1 000 000
5	–	100	4.994	1000	5.002	10 001	5.001	99 886	5.001	1 000 000
10	–	100	10.007	1000	10.004	10 000	10.003	100 022	10.001	990 709
20	–	100	19.999	1000	20.000	10 000	20.004	100 012	19.999	1 000 000
50	–	100	49.998	1000	49.999	10 001	50.001	100 125	50.003	1 000 000
80	–	100	80.004	1000	80.003	10 001	79.996	99 958	79.996	990 381

permittivity of the upper layer is 2, and the basement permittivities are varied discretely from 1 to 80. The resistivity is 5000 ohm-m in both layers. Figures 4b and 4c show the computed apparent resistivity and the apparent relative permittivity, respectively. When the upper layer shrinks to zero thickness on the left side of the figure, the earth becomes a homogeneous half-space with a true resistivity of 5000 ohm-m and with relative permittivities from 1 to 80. The computed apparent permittivities and the apparent resistivity are equal to the true values when the upper layer thickness becomes zero. At the right side of Figure 4a, where the upper layer is very thick, the earth again tends to homogeneity, in this case with an apparent resistivity of 5000 ohm-m and an apparent relative permittivity of 2, both being equal to the true values of the upper layer.

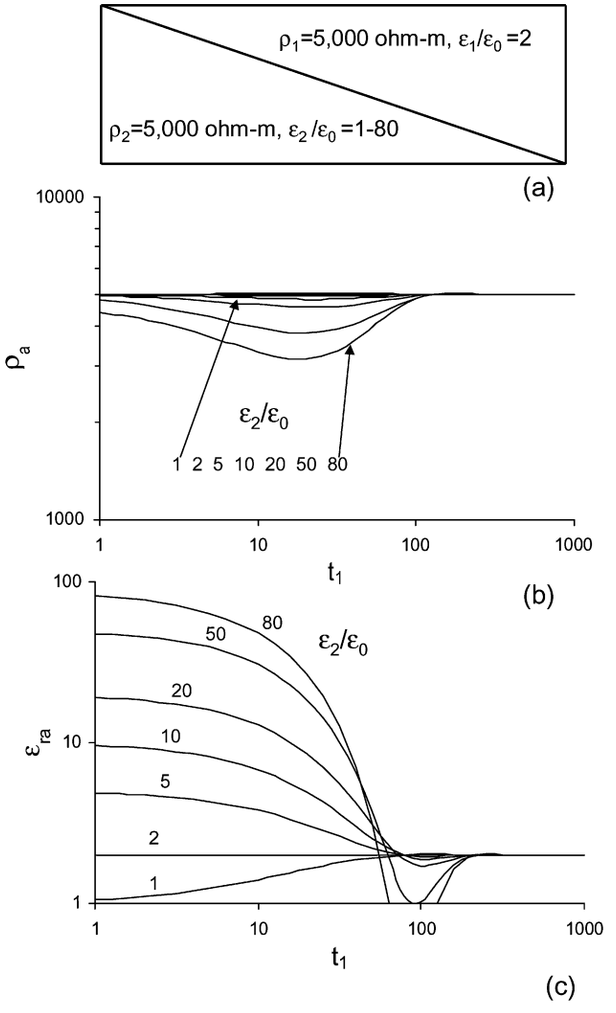

FIG. 4. (a) A continuous series of 1-D two-layer earth models where the thickness of the upper layer t_1 increases in small but discrete steps from left to right, and the interface between the two layers is shown as a sloping line drawn through these steps. The resistivity of both layers is 5000 ohm-m. The relative dielectric permittivity of the upper layer is 2, and the basement permittivities range from 1 to 80. This model was used to generate the in-phase and quadrature components at 105 000 Hz. These data were transformed to provide (b) the apparent resistivity ρ_a, and (c) the apparent relative permittivity ε_{ra}.

Between the left and right extremes of Figure 4, the apparent resistivity of Figure 4b is noticeably understated when $\varepsilon_r \geq 20$, for thicknesses t_1 in the middle range, even though the two layers have no resistivity contrast. Conversely, the permittivity behaves well except for the undershoot for large permittivity contrast when the upper layer is about 100 m thick, as shown in Figure 4c. This undershoot in the permittivity occurs approximately at one skin depth, which is 110 m for the frequency of 105 000 Hz. The resistivity and dielectric curves show, as they should, that the earth becomes a true homogeneous half-space when the permittivity of the basement and upper layer are the same ($\varepsilon_r = 2$), whereupon the apparent permittivity and apparent resistivity are both equal to the true values for all thicknesses of t_1.

Figure 5 is the same as Figure 4 except that the upper layer permittivities ε_r vary discretely from 1 to 80 and the basement is fixed at $\varepsilon_r = 2$. The effect of the dielectric permittivity is

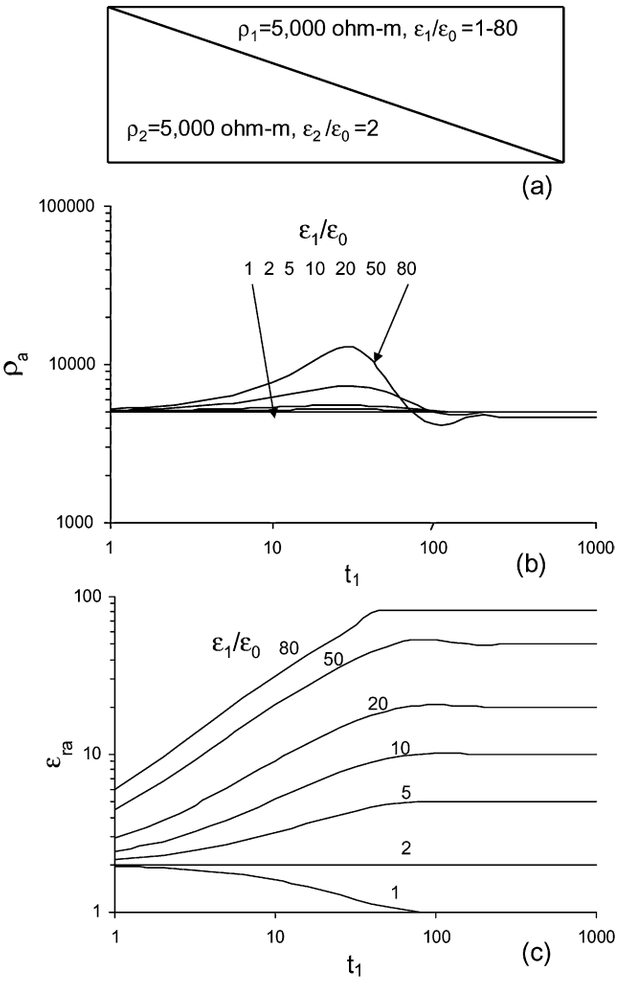

FIG. 5. (a) A continuous series of 1-D two-layer earth models where the thickness of the upper layer t_1 increases in discrete intervals from left to right. The resistivity of both layers is 5000 ohm-m. The relative dielectric permittivities of the upper layer range from 1 to 80, and the basement permittivity is 2. (b) The apparent resistivity ρ_a. (c) The apparent relative permittivity ε_{ra}.

to cause the apparent resistivity to exceed the true resistivity (Figure 5b). The apparent permittivity (Figure 5c) itself behaves well and is quite sensitive to the upper layer even when it is only 1-m thick.

Figure 6 shows the apparent resistivity, apparent permittivity, and the secondary field components I and Q for a two-layer model where the resistivity of the upper layer is 5000 ohm-m and the basement is 50 000 ohm-m. The permittivity of the basement is 1; the upper layer ranges between 1 and 80. A major overshoot occurs in the resistivity of Figure 6b in the vicinity of $t_1 = 15$m for the relative dielectric permittivity of 80. This large overshoot reflects the interplay of the in-phase response (Figure 6d) and the quadrature response (Figure 6e), and occurs where the in-phase is strongly negative and the quadrature relatively weak. Since conduction currents yield positive in-phase responses, the EM data of Figure 6d qualitatively implies that the conduction current is completely overwhelmed by the displacement current, and the computational results reflects this. This problem of overshoot does not exist for relative permittivities of 50 or less, and should not be a problem in most survey areas.

An overshoot occurs for the apparent permittivity in the midrange of the thickness axis t_1 in Figure 6c. The relative magnitude of the overshoot increases as the permittivity contrast decreases, being largest for $\varepsilon_r = 1$ where there is no permittivity contrast. This overshoot does not occur in the absence of a resistivity contrast between the layers (e.g., Figure 5c) or when the layering is reversed (Figure 7).

Figures 8 and 9 show the following about the response of a thin layer within a homogeneous half-space: (1) the thin layer is discernable by the apparent resistivity to a depth of about 10 m for this noise-free data regardless of whether the thin layer is relatively resistive (Figure 8b) or conductive (Figure 9b); (2) the thin layer is discernable by the apparent relative permittivity to a depth of approximately 80 m regardless of whether it is relatively resistive (Figure 8c) or conductive (Figure 9c); (3) the apparent relative permittivity may undershoot (Figure 8c) or overshoot (Figure 9c) for small values of the permittivity contrast; and (4) even when there is no permittivity contrast between the thin layer and the host, the true relative permittivity of 2 cannot be obtained because of the impact of the resistivity contrast between the thin layer and the host.

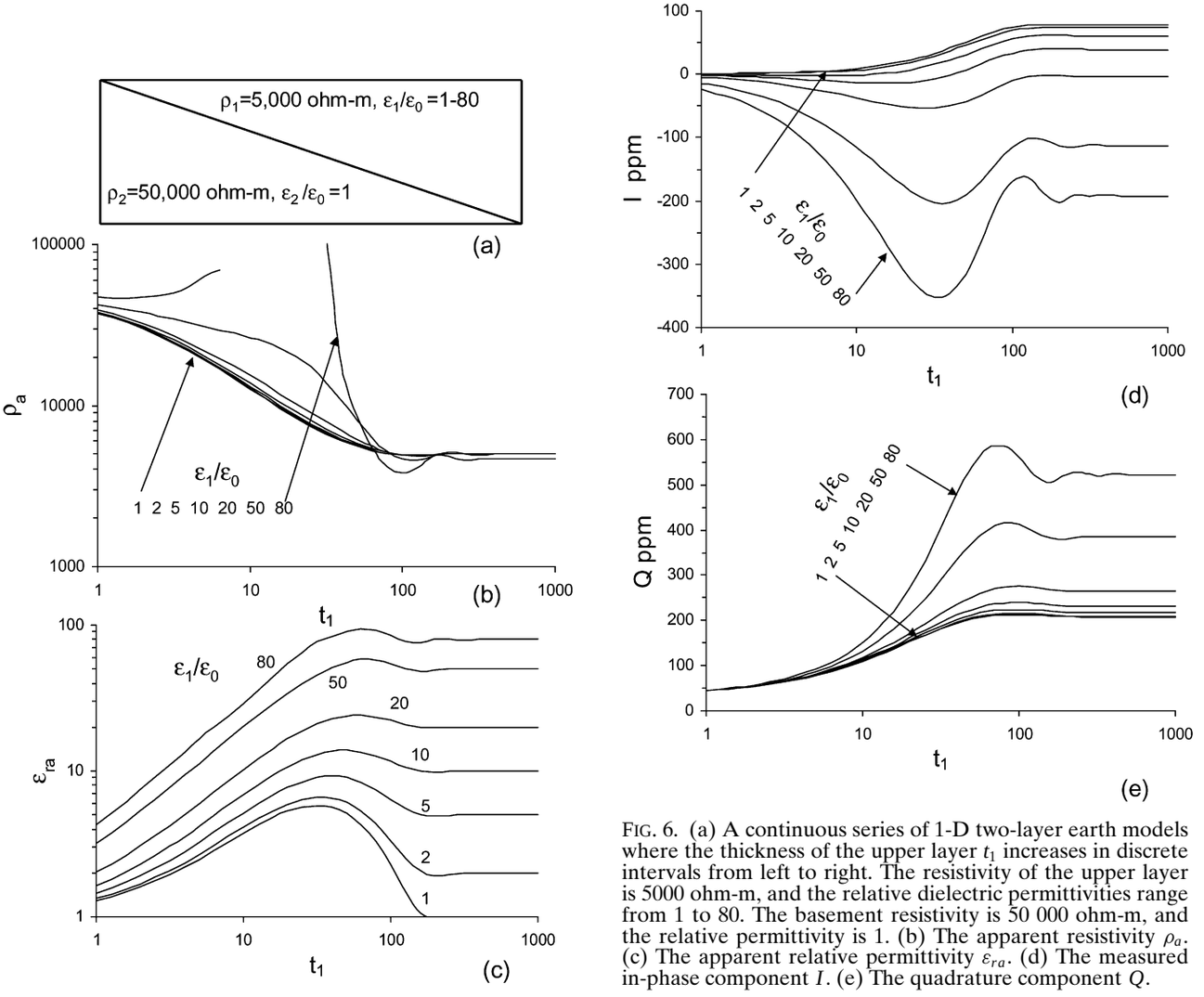

FIG. 6. (a) A continuous series of 1-D two-layer earth models where the thickness of the upper layer t_1 increases in discrete intervals from left to right. The resistivity of the upper layer is 5000 ohm-m, and the relative dielectric permittivities range from 1 to 80. The basement resistivity is 50 000 ohm-m, and the relative permittivity is 1. (b) The apparent resistivity ρ_a. (c) The apparent relative permittivity ε_{ra}. (d) The measured in-phase component I. (e) The quadrature component Q.

The above limitation of 80 m on the detection depth of dielectric polarization in these two thin-layer models may be compared with the capability of the DIGHEM helicopter EM system to detect a thin nondielectric conductive layer at more than twice this depth, as shown by Huang and Fraser (1996).

TEST ON REAL DATA

The dielectric resistivity algorithm was tested on DIGHEM survey data from an area in northern Canada (Figure 10a) where the ground resistivity is generally greater than 5000 ohm-m. The effect of displacement currents were believed to be significant because many negative in-phase responses were observed at 56 000 Hz, this being the highest frequency of the system used in this survey. The apparent resistivity $\rho_a(\varepsilon = 0)$ as shown in Figure 10b is computed from the in-phase and quadrature data at 56 000 Hz using the pseudolayer half-space model (Figure 1b) and ignoring the effects of displacement currents. The apparent resistivity over the central lake, with its surface frozen, is more than 10 000 ohm-m. This resistivity is overstated because displacement currents are not taken into account in the calculation of the resistivity.

The apparent resistivity $\rho_a(\varepsilon = \varepsilon_r\varepsilon_0)$ computed with the permittivity-resistivity algorithm is shown in Figure 10c. Low resistivity values outline the central lake very well. The apparent resistivity over the lake is about 3000 ohm-m, suggesting that the lake is probably quite shallow since the resistivity of the fresh waters of northern Canada should be of the order of 300 ohm-m (McNeill, 1980). The apparent permittivity is

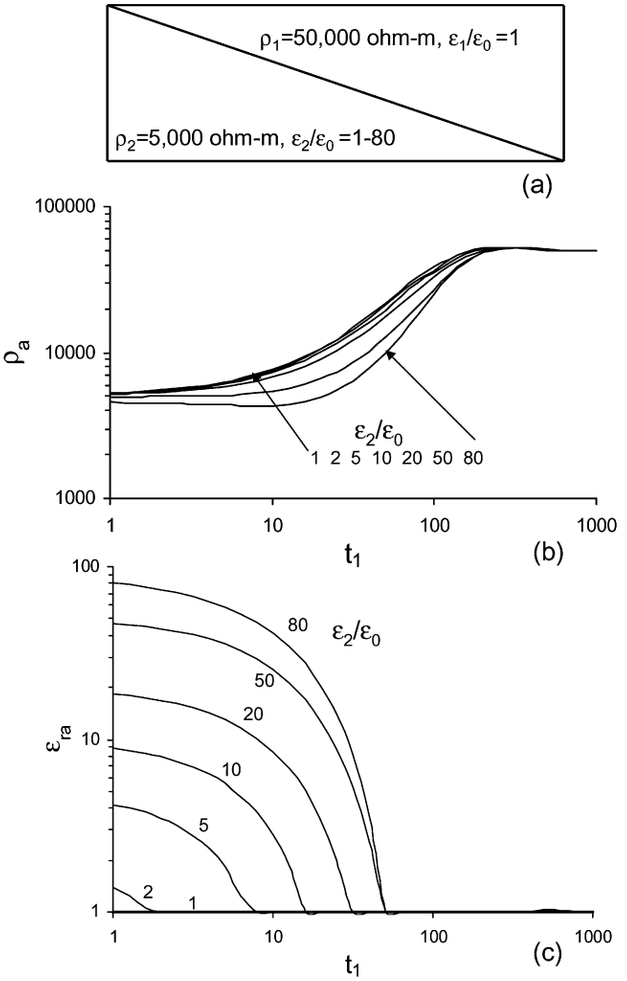

FIG. 7. (a) A continuous series of 1-D two-layer earth models where the thickness of the upper layer t_1 increases in discrete intervals from left to right. The resistivity of the upper layer is 50 000 ohm-m, and the relative permittivity is 1. The basement resistivity is 5000 ohm-m, and the relative dielectric permittivities range from 1 to 80. (b) The apparent resistivity ρ_a. (c) The apparent relative permittivity ε_{ra}.

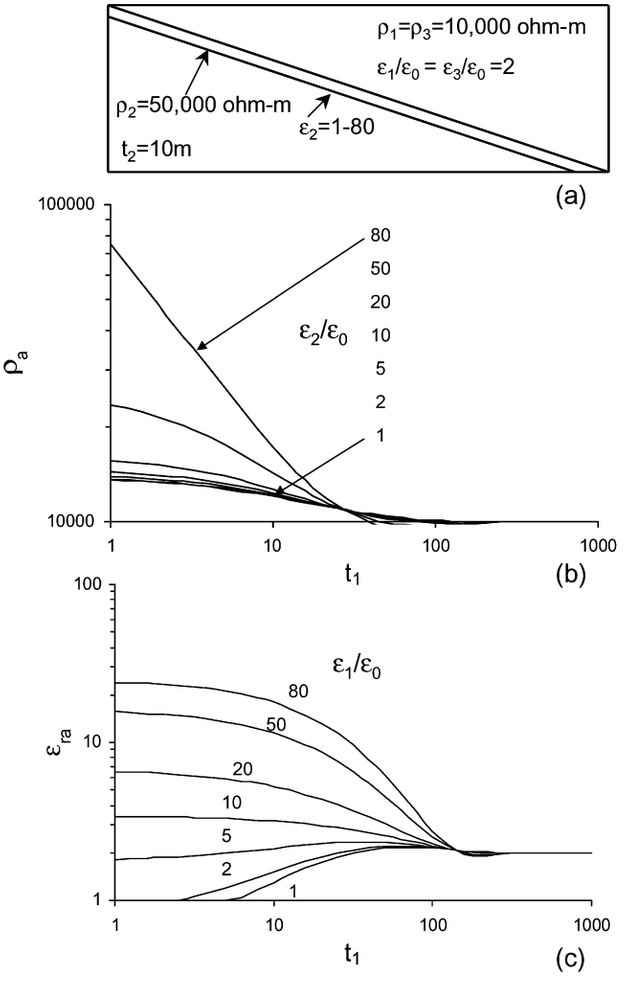

FIG. 8. (a) A continuous series of 1-D three-layer earth models where the thickness of the upper layer t_1 increases in discrete intervals from left to right. Layer 2 is 10-m thick with a resistivity of 50 000 ohm-m and with relative permittivities ranging from 1 to 80. The host (layers 1 and 3) has a resistivity of 10 000 ohm-m and a relative permittivity of 2. (b) The apparent resistivity ρ_a. (c) The apparent relative permittivity ε_{ra}.

shown in Figure 10d. The permittivity highs correspond to the lakes. Also, there are some features on the permittivity map that cannot be seen on the resistivity maps. Unfortunately, we do not have the ground truth needed to identify the cause of these features.

A profile across A-B of Figure 10 is illustrated in Figure 11 and shows the in-phase and quadrature data at 56 000 Hz, the apparent resistivities for $\varepsilon = 0$ and $\varepsilon = \varepsilon_r \varepsilon_0$, and the apparent relative permittivity ε_r. The apparent resistivity obtained from the permittivity-resistivity algorithm is 2800 ohm-m over the center of the lake, while the apparent permittivity is 65. We can obtain an indication of the reasonableness of these figures by modeling.

Figure 12a presents a three-layer model simulating the above example for the frozen lake in northern Canada. The upper layer represents ice 1-m thick overlying a middle layer of unfrozen lake water. The bottom layer is the resistive bedrock under the lake. Figures 12b and 12c are the apparent resistivity and apparent permittivity as a function of the water thickness t_2. As the model lake gets deeper, the apparent resistivity and permittivity approach the true values of the water. In Figure 11, we noted that the apparent permittivity at the center of the lake is 65. From Figure 12c, a permittivity of 65 would indicate a water thickness of 3 m. The 3-m water thickness then would give an apparent resistivity of 2100 ohm-m (Figure 12b). This is not an exact match to the apparent resistivity of 2800 ohm-m, but it is close. Without ground truth, this exercise simply serves as an illustration of the interplay of the parameters of the dielectric-resistivity technique.

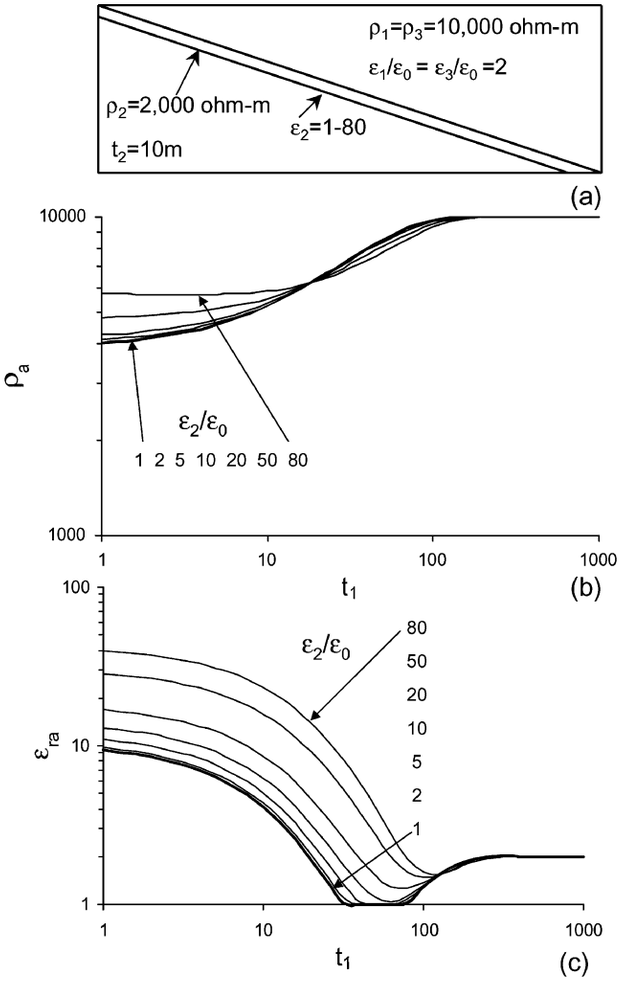

FIG. 9. (a) A continuous series of 1-D three-layer earth models where the thickness of the upper layer t_1 increases in discrete intervals from left to right. Layer 2 is 10-m thick with a resistivity of 2000 ohm-m and with relative permittivities ranging from 1 to 80. The host (layers 1 and 3) has a resistivity of 10 000 ohm-m and a relative permittivity of 2. (b) The apparent resistivity ρ_a. (c) The apparent relative permittivity ε_{ra}.

CONCLUSIONS

An analysis has been made of the feasibility of dielectric permittivity and resistivity mapping using a high-frequency airborne EM system. The displacement current caused by dielectric permittivity decreases the in-phase component and increases the quadrature component from the conduction current. This produces an unwarranted increase in the apparent resistivity, if the permittivity is neglected, when computing the resistivity from the preferred pseudolayer half-space model.

A new algorithm has been developed for transforming the in-phase and quadrature components into the apparent relative dielectric permittivity and apparent resistivity. The permittivity can be well resolved in a resistive environment. However, the solution for the permittivity cannot be obtained when the resistivity is lower than about 800 ohm-m for the 105 000 Hz of the $\text{DIGHEM}^{\text{V}}_{\text{Res}}$ system.

The behavior of the apparent permittivity and apparent resistivity for some two-layer and three-layer models reveals that the depth of detection of a dielectric polarizable layer may be as high as 80 m under favorable conditions. In certain layered earth cases, the permittivity-resistivity algorithm may give misleading results due to an overshoot or undershoot in the computed parameters.

Permittivity-resistivity mapping may be useful in civil engineering and for environmental and geological mapping. The method in particular may be useful for the mapping of hazardous waste sites where some contaminants may have little effect on the observed resistivity but a large effect on the observed permittivity.

ACKNOWLEDGMENTS

Appreciation is expressed to Richard Smith and Peter Wolfgram for their helpful suggestions, and to Fugro Airborne Surveys for permission to publish this paper. We are grateful to Tahera Corporation (formerly Lytton Minerals Limited) for permission to use their DIGHEM survey data to show the results from the analytic techniques presented in this paper.

REFERENCES

Fraser, D. C., 1972, A new multicoil aerial electromagnetic prospecting system: Geophysics, **27**, 518–537.

——— 1978, Resistivity mapping with an airborne multicoil electromagnetic system: Geophysics, **43**, 144–172.

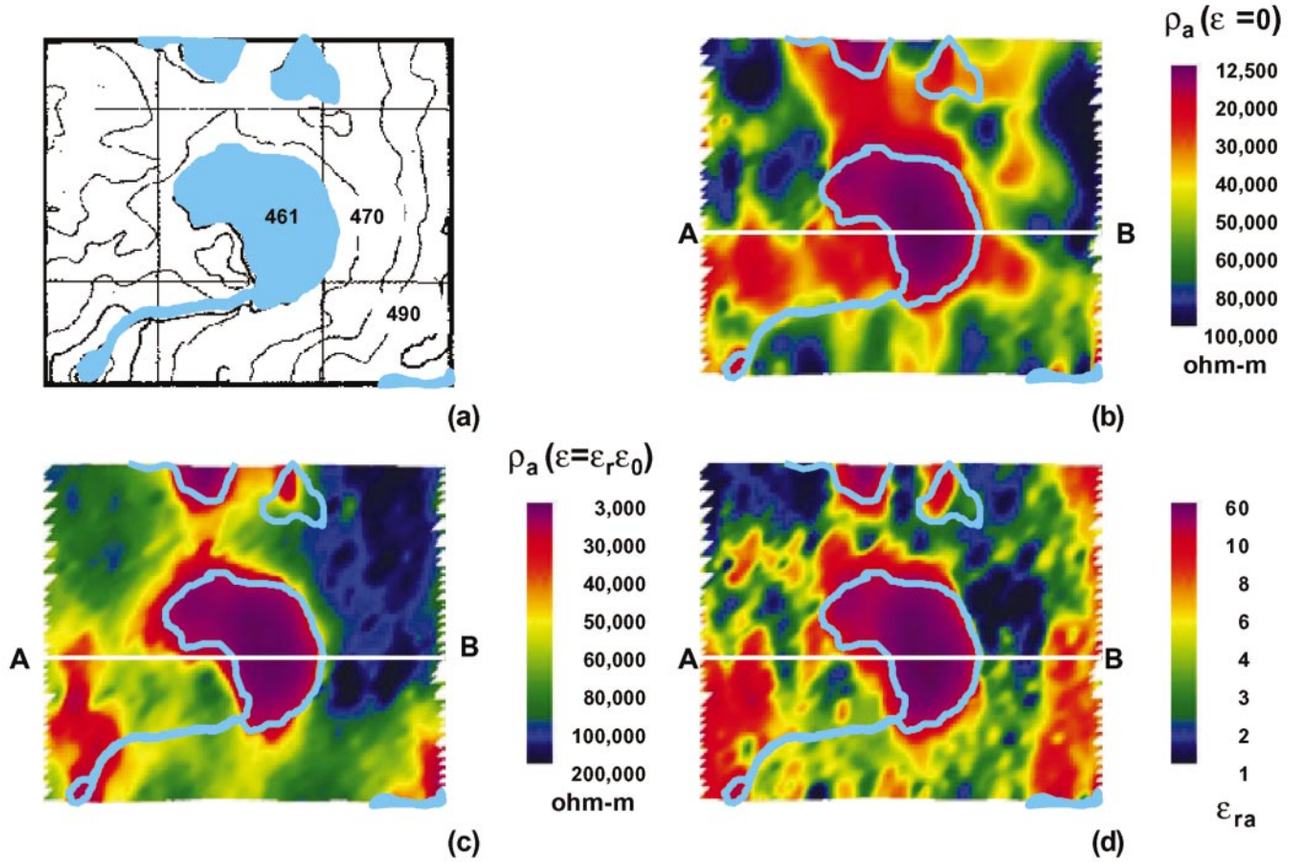

FIG. 10. (a) The survey area with lakes and a river shown in blue. (b) The apparent resistivity at 56 000 Hz assuming the absence of dielectric polarization (i.e., $\varepsilon = 0$). (c) The apparent resistivity obtained from the permittivity-resistivity algorithm assuming $\varepsilon = \varepsilon_{ra}\varepsilon_0$. (d) The apparent relative permittivity ε_{ra}. Equal area color distributions were used for (b) and (c), rather than a common color bar, to avoid a bias which might visually favor one parameter over the other.

Fraser, D. C., Stodt, J. A., and Ward, S. H., 1990, The effect of displacement currents on the response of a high-frequency helicopter electromagnetic system; *in* Ward, S. H., Ed., Geotechnical and Environmental Geophysics: II, Environmental and Groundwater: Soc. Expl. Geophysics, 89–96.

Frischknecht, F. C., 1967, Fields about an oscillating magnetic dipole over a two-layer earth and application to ground and airborne electromagnetic surveys: Quarterly of the Colorado School of Mines, **62**, no. 1, 326.

Grant, F. S., and West, G. F., 1965, Interpretation theory in applied geophysics: McGraw-Hill.

Huang, H., and Fraser, D. C., 1996, The differential parameter method for multifrequency airborne resistivity mapping: Geophysics, **61**, 100–109.

——— 2000, Airborne resistivity and susceptibility mapping in magnetically polarizable areas: Geophysics, **65**, 502–511.

——— 2001, Mapping of the resistivity, susceptibility and permittivity of the earth using a helicopter-borne electromagnetic system: Geophysics, **66**, 148–157.

Huang, H., Hodges, G., and Fraser, D. C., 1998, Mapping dielectric permittivity and resistivity using high frequency helicopter-borne EM data: 68th Ann. Internat. Mtg., Soc. Expl. Geophys., Expanded Abstracts, 817–820.

Lawson, C. L., and Hanson, R. J., 1974, Solving least-squares problems: Prentice Hall, Inc.

Lysne, P. C., 1983, A model for the high-frequency electrical response of wet rocks: Geophysics, **48**, 775–786.

Lytle, J. R., Lager, D. L., and Laine, E. F., 1976, Subsurface probing by high-frequency measurements of the wave tilt of electromagnetic surface waves: IEEE Trans. Geosci. Electr., **14**, 244–249.

McNeill, J. D., 1980, Electrical conductivity of soils and rocks: Geonics Ltd. Tech. Note TN-5.

Menke, W., 1984, Geophysical data analysis—Discrete inverse theory: Academic Press, Inc.

Olhoeft, G. R., 1986, Direct detection of hydrocarbon and organic chemicals with ground penetrating radar and complex resistivity: Proc. National Water Well Assn./Am. Petr. Inst. Conf. on Petroleum Hydrocarbons and Organic Chemicals in Ground Water, 284–304.

Sengpiel, K. P., 1988, Approximate inversion of airborne EM data from a multilayered ground: Geophys. Prosp., **36**, 446–459.

Sinha, A. K., 1977, Influence of altitude and displacement currents on plane-wave EM fields: Geophysics, **42**, 77–91.

Song, Y., Morrison, F. H., and Lee, H. K., 1997, High frequency electromagnetic impedance for subsurface imaging: Proc. Symp. on the Application of Geophysics to Engineering and Environmental Problems, **2**, 761–772.

Stewart, D. C., Anderson, W. L., Grover, T. P., and Labson, V. F., 1994, Shallow subsurface mapping by electromagnetic sounding in the 300 kHz to 30 MHz range: Model studies and prototype system assessment: Geophysics, **59**, 1201–1210.

Wait, J., 1984, Relaxation phenomena and induced polarization: Geoexplor., **22**, 107–127.

Ward, S. H., 1967, Electromagnetic theory for geophysical applications, *in* Ward, S. H., Ed., Mining geophysics, II: Theory: Soc. Expl. Geophys., 13–196.

Ward, S. H., and Hohmann, G. W., 1988, Electromagnetic theory for geophysical applications, *in* Nabighian, M. N., Ed., Electromagnetic methods in applied geophysics, I: Theory: Soc. Expl. Geophys., 130–311.

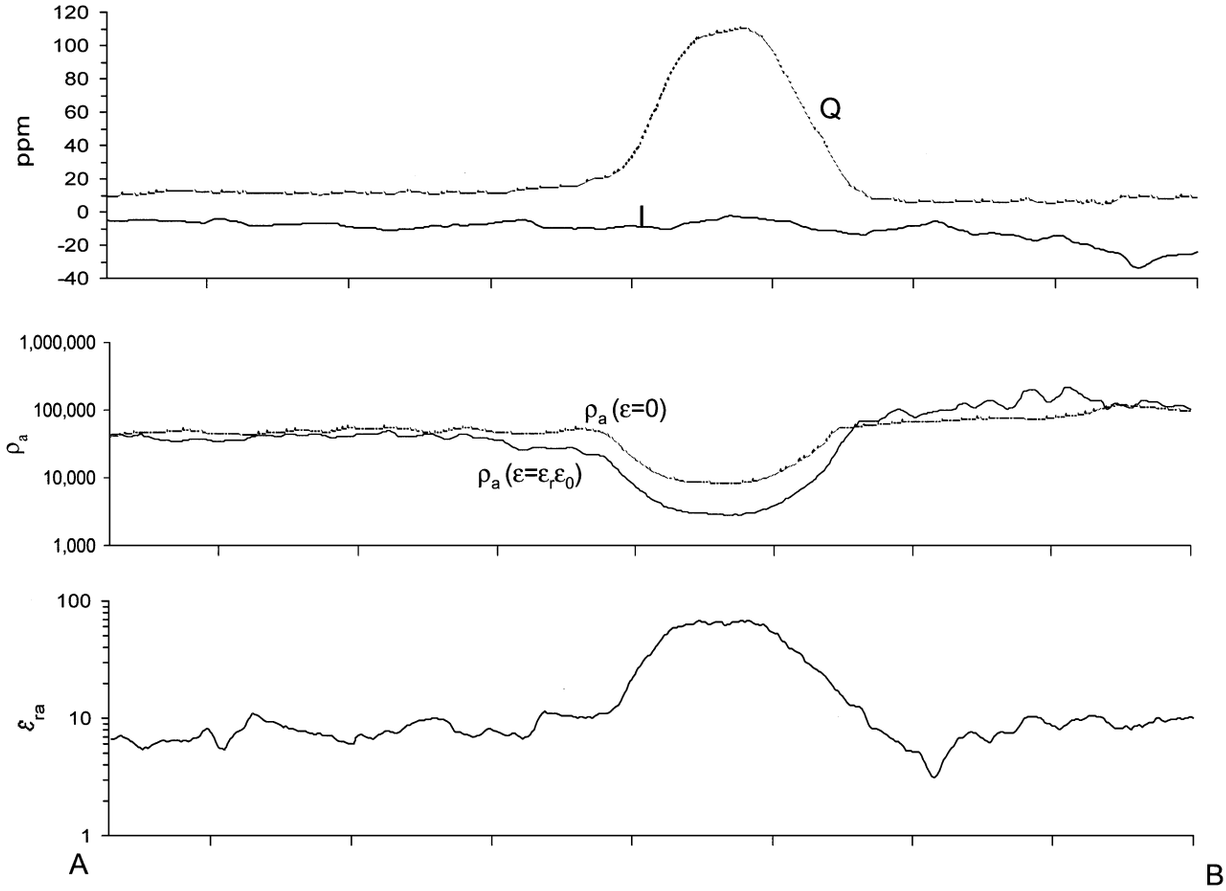

FIG. 11. A profile across A-B of Figure 10 showing the in-phase I and quadrature Q data at 56 000 Hz, the apparent resistivity ρ_a for $\varepsilon = 0$ and for $\varepsilon = \varepsilon_{ra}\varepsilon_0$, and the apparent permittivity ε_{ra}.

APPENDIX

THE TABLE LOOKUP PROCEDURE

The dielectric permittivity and conductivity of a dielectric conductive half-space are obtained by transforming the in-phase and quadrature responses using a table lookup program that yields the same results as a one-layer inversion.

We create two arrays of **M** and **N,** in which **M** contains m in-phase data ranging from $-19\,000$ to 80 000 ppm and **N** contains n quadrature data from 500 to 100 000 ppm, as shown in Figure 3, where $M' = M + 20\,000$. **M** and **N** can be written in general as $\mathbf{M} = [M_1, M_2, \ldots, M_m]$ and $\mathbf{N} = [N_1, N_2, \ldots, N_n]$. Data M_i, N_j are equally spaced logarithmically. Given a frequency f, flying height h, and coil separation s, M_i and N_j can be used as in-phase and quadrature data to input to an inversion program based on a homogeneous half-space model. The inversion yields a resistivity ρ (or conductivity σ) and relative permittivity ε_r for each pair of M_i and N_j. Scanning through $i = 1, \ldots, m$, and $j = 1, \ldots, n$, we generate two $m \times n$ tables of $\mathbf{A} = \{\alpha_{ij}\}$ and $\mathbf{B} = \{\beta_{ij}\}$, where $\alpha_{ij} = \omega^2 \varepsilon_{ij} \mu_0 h^2$ and $\beta_{ij} = \omega \sigma_{ij} \mu_0 h^2$ are associated with data M_i and N_j. Having a pair of in-phase and quadrature data (M_i, N_j), we can directly obtain α_{ij} and β_{ij}, and thence the resistivity ρ and permittivity ε_r, according to the indexes i and j. In general, α and β can be obtained by using a 2-D interpolation scheme from any M and N within the given ranges. In this paper, the following interpolation equation is used,

$$z(M, N) \approx \sum_{j=1}^{n} \sum_{i=1}^{m} \prod_{\substack{k=1 \\ k \neq i}}^{m} \left(\frac{M - M_k}{M_i - M_k} \right) \prod_{\substack{l=1 \\ l \neq j}}^{n} \left(\frac{N - N_l}{N_j - N_l} \right) z_{ij},$$

where z_{ij} stands for either α_{ij} or β_{ij} at a node, and $z(M, N)$ for the interpolated value for a given in-phase M and quadrature N.

Traditional inversion techniques for solving nonlinear inverse problems are used to obtain the resistivity ρ (or conductivity σ) and relative permittivity ε_r. An objective function is minimized subject to fitting the data in the least squares sense. More details can be found in Lawson and Hanson (1974) and Menke (1984). The forward solution of a layered half-space earth for dipole source excitation is given by Ward (1967), Frischknecht (1967), and Ward and Hohmann (1988), among many others.

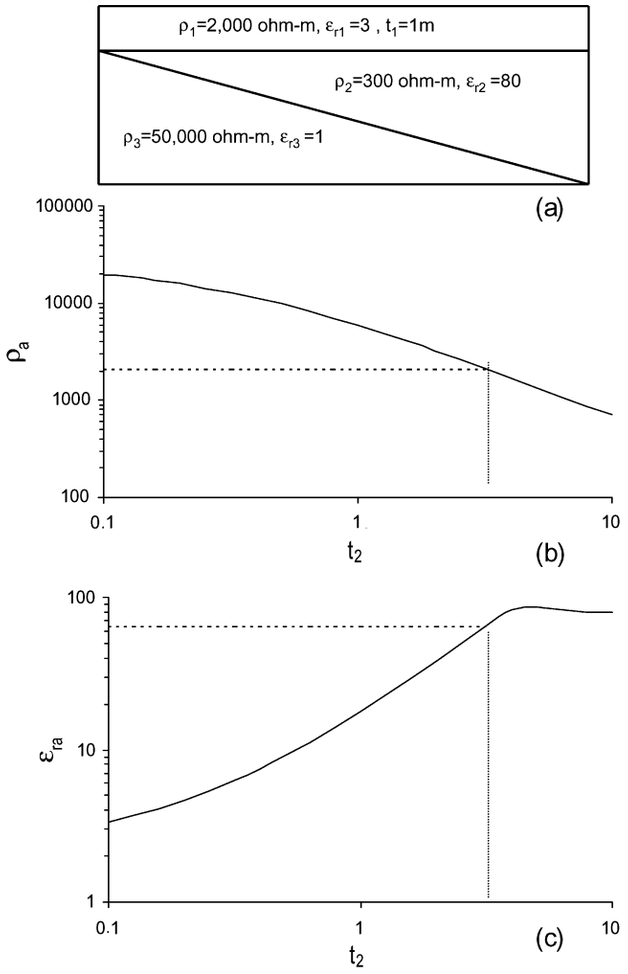

FIG. 12. The apparent resistivity ρ_a and apparent permittivity ε_{ra} of a three-layer model simulating the lake example of Figure 11.